Proceedings of the Twenty-seventh (2017) International Ocean and Polar Engineering Conference **www.isope.org**
San Francisco, CA, USA, June 25-30, 2017

ISBN 978-1-880653-97-5; ISSN 1098-6189

Tsunami detection by High Frequency Radar using a Time-Correlation Algorithm: performance analysis based on data from a HF radar in British Columbia

Charles-Antoine Guérin[1], *Stéphan T. Grilli*[2], *Patrick Moran*[2], *Annette Grilli*[2] *and Tania Insua*[3]
(1) Université de Toulon, CNRS, Aix Marseille Université, IRD MIO UM 110, La Garde, France
(2) Department of Ocean Engineering, University of Rhode Island, Narragansett, RI, USA
(3) Ocean Networks Canada (ONC), Victoria, BC.

ABSTRACT

A High-Frequency (HF) radar was installed by Ocean Networks Canada in Tofino, BC, to detect tsunamis from far- and near-field sources on the Pacific Ocean side of Vancouver Island; in particular, from seismic sources in the Cascadia Subduction Zone. Based on a classical analysis of the Doppler spectrum, this HF radar can measure ocean surface currents up to a 85-110 km range depending on sea state. However, an inherent limitation of detection of small and short-lived tsunami currents is the conflicting requirement for short integration time and sufficient accuracy (resolution) of the Doppler spectra. This limits a direct tsunami detection typically to shallow water areas over the continental shelf where tsunami currents have become sufficiently strong due to wave shoaling.

To overcome this limitation, the authors have recently proposed a new detection method, referred to as "Time-Correlation Algorithm (TCA)", that does not require inverting Doppler spectra for the tsunami currents and can thus potentially detect an approaching tsunami in deeper water, beyond the continental shelf. This algorithm is based on computing space-time correlation of the raw radar signal in different radar cells aligned along precomputed tsunami wave rays, and time-shifted by the precomputed tsunami propagation time between cells. A change in pattern of such correlations indicates the presence of a tsunami. They validated the TCA with numerical simulations for both idealized (Grilli et al., 2016a) and realistic (Grilli et al., 2016b, 2017) tsunami wave trains and seafloor bathymetry, using data simulated with a radar simulator.

Here, the TCA is for the first time applied to actual radar data measured with the ONC WERA HF radar and numerically modified by a synthetic tsunami current. Using a state-of-the-art long wave model we perform tsunami simulations with realistic source and bathymetry, and combine the resulting currents with the background currents and radar backscattered signal measured by the HF radar system. This combination makes it possible to evaluate the performance of the proposed TCA detection algorithm, based on an experimental rather than numerically simulated, data set of radar signal. Our findings confirm that an actual detection can be achieved beyond the continental shelf, where tsunami currents are small (as low as 5 cm/s), in deeper water than when using an algorithm based on a direct inversion of currents from the measured radar Doppler spectra.

INTRODUCTION

The use of shore-based High Frequency (HF) radars to detect incoming tsunami waves was proposed almost 40 years ago by Barrick (1979) and, more recently, was supported by numerical simulations (see, e.g., (Lipa et al., 2006), (Heron et al., 2008), (Dzvonkovskaya et al., 2009), (Gurgel et al., 2011) and (Grilli et al., 2016a)), and by HF radar measurements of the Tohoku 2011 tsunami made in Japan (Hinata et al., 2011; Lipa et al., 2011, 2012), in Chile ((Dzvonkovskaya, 2012)), and in Hawaii ((Benjamin et al., 2016)). HF radars are routinely used to estimate surface currents based on the analysis of the Doppler spectrum over a grid of radar cells, covering a sweep area of tens to hundreds of kms, and new radars have been installed or existing radar used as a means of detecting tsunami currents as well. To do so, tsunami detection algorithms were proposed (see some of the above studies), based on identifying the oscillatory nature of tsunami currents, in space and/or time in the radar measurements. There are, however, some intrinsic limitations to this detection method. In order to be detectable, the magnitude of the tsunami current should be larger than the threshold of accuracy of the Doppler-based estimation. This accuracy depends mainly on the radar frequency and integration time used to compute the Doppler spectrum. Estimating small currents requires large integration times, but this is in contradiction with the oscillatory nature of tsunami currents, as a large integration time will cause averaging and significant decrease of these currents, which will become less measurable. Hence, the integration time must remain short enough (up to a few minutes) to avoid averaging out the tsunami induced current, which will reduce the resolution and detection threshold of the Doppler-based methods. In practice, this limits a direct detection of tsunami currents by way of Doppler shifts to the continental shelf where currents have become sufficiently large due to shoaling; hence, this also means small warning times, unless there is a very wide shelf.

Recently, (Grilli et al., 2016a,b, 2017) proposed a new detection method, which we refer to as the "Time Correlation Algorithm" (TCA), which does not require inverting Doppler spectra for the currents, but is based on the space-time correlation properties of the radar signal along pre-computed tsunami wave rays. By performing numerical radar and tsunami simulations for both idealized (Grilli et al., 2016a) and realistic (Grilli et al., 2016b, 2017) seafloor bathymetry, we found that the TCA detection algorithm could be applied beyond the continental shelf,

in deeper water, where tsunami currents are small (a few cm/s).

Here, for the first time, we report on the implementation of the TCA using actual measured radar data measured off of the Pacific Ocean side of Vancouver Island (radar deployed at Tofino, BC), together with simulated tsunami currents using a state-of-the-art tsunami propagation model. As it has been customary in other related works, we superimpose the effect of tsunami currents on the measured radar signal by the introduction, in each radar cell, of a phase shift depending on a current memory term (see details below). We show results for a Mw 9.1 far-field seismic source in the Semidi Subduction Zone (SSZ; Fig. 1). The numerical generation of a tsunami for this source was presented elsewhere and we refer to (Grilli et al., 2016b, 2017) for details.

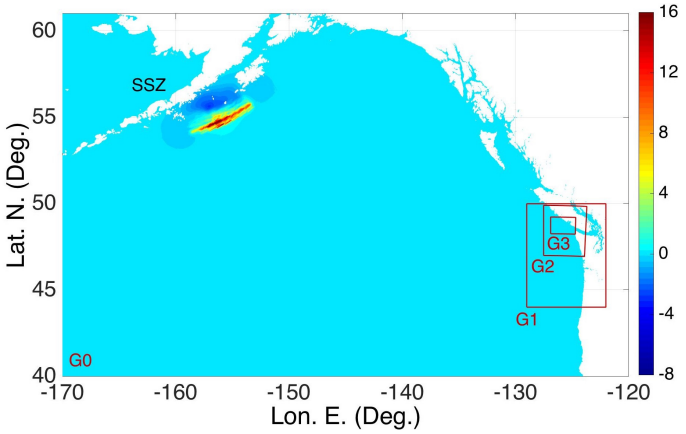

Fig. 1: Zoom-in on area of the Pacific Ocean covered by the 2 arc-min grid G0, with initial surface elevation (color scale in meter) of the M_w 9.1 SAFRR seismic source in the Semidi Subduction Zone (SSZ); boundaries of nested model grids off of Vancouver Island, BC, are shown as black boxes: G1 (0.6 arc-min), G2 (270 m), and G3 (90 m)

WERA HF RADAR SYSTEM USED IN THIS WORK

To mitigate the elevated tsunami hazard along the shores of Vancouver Island in British Columbia, Canada, Ocean Networks Canada (ONC) has been developing a Tsunami Early Warning System combining instrument deployment on the seafloor as part of their Neptune Observatory, and a shore-based High-Frequency (HF) radar installed near Tofino (BC) (Fig. 2), which has been operational since April 2016. This WERA HF radar, with carrier frequency f_{EM} = 13.5 MHz, can detect and estimate ocean radial currents up to a 85-110 km range depending on sea state, as the propagation losses increases with sea surface roughness. An example of a typical current map is shown in Fig. 2.

The radar sweep area is outlined in Fig. 4 and is covered by radar cells, within which the received radar signal is averaged. The cells all have a radial length $\Delta R = 1.5$ km and an angular opening $\Delta\phi_r = 1$ degree in the azimuthal direction; the detection sector of the sweep area is 120 degree, implying that cells are 1.48 km wide at a 85 km range and narrower closer to the radar (cell area: $\Delta\mathbb{S} = R\Delta R\Delta\phi_r$ increases with range). The orientation of the radar array of 12 antennas (275 deg. from N, clockwise; centered at 49° 4' 24.82" N, 125° 46' 11.55" W; Fig. 2) is such that one side of the sweep area boundary is nearly parallel to the coastline southeast of Tofino, and the array length (110 m) allows for approximately a 12 degree azimuthal resolution. In the direction finding algorithm, as the radar signal is processed for overlapping angular windows, surface currents are estimated in a larger number of radar cells with a 1 degree azimuthal resolution.

Fig. 2: The ONC WERA HF radar site in Tofino, BC.

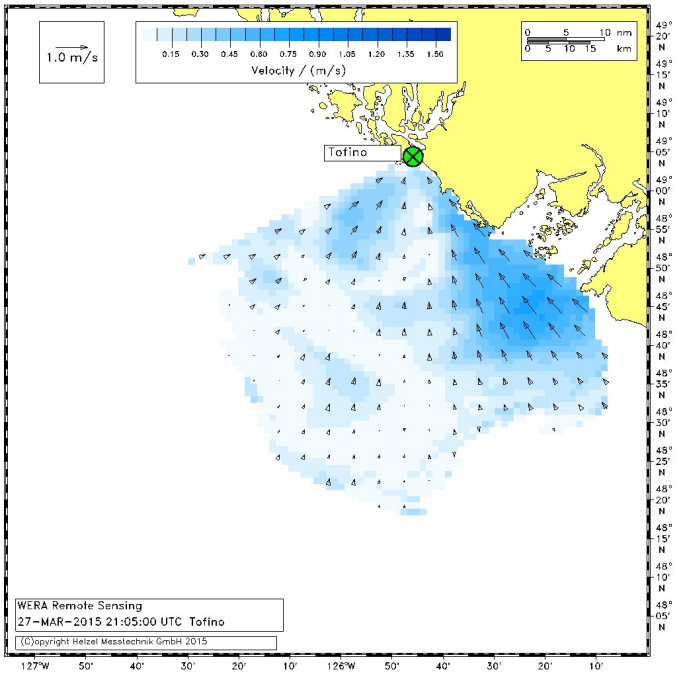

Fig. 3: Typical map of radial surface currents measured by the WERA HF radar installed in Tofino, BC, by inversion of the Doppler spectra.

THE TIME-CORRELATION ALGORITHM (TCA)

According to first-order Bragg theory, the complex backscattered signal received at time t for a given radar cell p is of the form:

$$\mathrm{V}_q(t) = \alpha^+ \, e^{-2i\pi f_B t} + \alpha^- \, e^{+2i\pi f_B t} \tag{1}$$

where $\alpha^{\pm}$ are constant complex coefficients function of sea state, range, and radar calibration, and $f_B = \sqrt{g/(\pi\lambda_{EM})}$ is the Bragg frequency (λ_{EM} is the electromagnetic wavelength). In the presence of a constant current U, the complex radar signal experiences a Doppler frequency shift $f_U = -2U/\lambda_{EM}$ and is thus multiplied by a complex exponential $e^{2i\pi f_U t}$. For a variable current in time, $U(t)$, the Doppler frequency shift is obtained through the integration of the instantaneous Doppler frequency $f_U(t) = -2U(t)/\lambda_{EM}$, and the radar time series is multiplied by the complex exponential $e^{iM(t)}$, where

$$M(t) = -\frac{4\pi}{\lambda_{EM}} \int_{-\infty}^{t} U(t')dt' \tag{2}$$

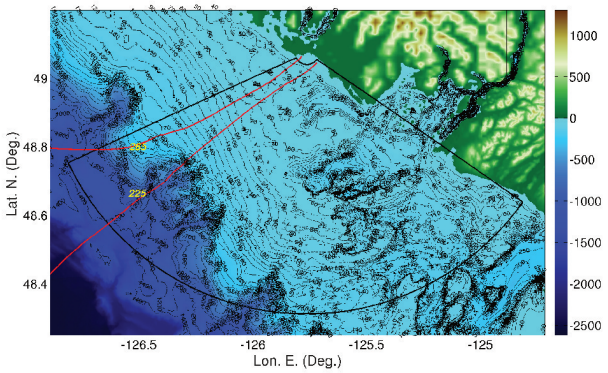

Fig. 4: Footprint of ONC WERA HF radar sweep area off of Tofino, BC, with the marked trace (red solid lines) of 2 wave rays corresponding to tsunami sources originating from the North-West (285) and South-West (225) direction.

In the presence of a tsunami wave train, we therefore have the modified radar signal:

$$\mathrm{V}_q(t) = \left(\alpha^+ \, e^{-2\mathrm{i}\pi f_B t} + \alpha^- \, e^{+2\mathrm{i}\pi f_B t}\right) e^{\mathrm{i}M(t)} \tag{3}$$

The additional phase shift is sometimes referred to as the "memory term", as it integrates the past values of the current.

Now, the presence of a tsunami wave train within a given sea state manifests itself as a slowly varying induced orbital current, proportional to the local wave elevation, which propagates with the tsunami phase speed. The main idea underlying the TCA is to take advantage of the unique large scale coherency of this tsunami-induced current, to identify its occurence in the radar signal through its effect on the memory term. As the tsunami wave train propagates over large distances with little deformation, along wave rays and at a known (depth-dependent) phase speed (approximated by $c = \sqrt{gh}$, with h the local depth), the induced currents at successive locations along such rays should be strongly correlated. More specifically, we expect the strongest correlation to occur between the current $U_p(t)$ at cell p and the time-shifted current $U_q(t+t_{pq})$ at cell q, where t_{pq} is the tsunami travel time from cell p to cell q. This property carries over the memory term and therefore also to the radar signal itself. The TCA thus calculates correlations of the complex backscattered radar signal time series $(V_p(t), V_q(t+t_{pq}))$ received from 2 given cells (p,q), located along the same tsunami ray:

$$C_{pq}(\tau;t) = \left|\mathrm{corr}\{\mathrm{V}_p(t+\tau-t_p), \mathrm{V}_q(t-t_q)\}\right|, \tag{4}$$

where t_p and t_q are the travel times from some reference cell p_0 to the cells p and q, respectively, and τ an additional time lag.

With this definition, the maximum correlation is expected at $\tau = 0$, that is when the time lag between the two signals is $t_{pq} = t_q - t_p$. Hence, when a change in pattern of correlations C_{pq} occurs near $\tau = 0$, this indicates that a tsunami is propagating through the radar sweep area. In practice, the ensemble average is obtained through a temporal average with a running time window:

$$C_{pq}(\tau;t) = \left| \frac{1}{T_c} \int_{t-\frac{T_c}{2}}^{t+\frac{T_c}{2}} \mathrm{V}_p(t'+\tau-t_p)\, \mathrm{V}_q^*(t'-t_q)\, \mathrm{d}t' \right| \tag{5}$$

with T_c the length of the time window, which should be sufficiently large to capture the oscillations of the tsunami current, that is at least one-third to one-half the tsunami dominant period T_t.

TSUNAMI SIMULATIONS

Time series of tsunami currents are obtained in each radar cell from results of simulations performed with the state-of-the- art long wave model FUNWAVE-TVD (Shi et al. 2012; Kirby et al. 2013a), by one-way coupling, using nested grids G0, G1, G2, G3 (Fig. 1). Time series of simulated tsunami horizontal currents $\mathbf{u}_t$ are projected in the radar radial direction $\mathbf{R}$ as $U_{tr} = \mathbf{u}_t \cdot \mathbf{R}$ and spatially-averaged over individual radar cells covering the radar sweep area. Here, we only detail results obtained for a M_w 9.1 far-field seismic source located in the Semidi Subduction zone (SSZ; Fig. 1), but simulations were also performed for large seismic sources in the Cascade Subduction Zone (Insua et al., 2015). Figure 5 shows 4 snapshots of the radial tsunami current magnitude computed over the radar sweep area for the SSZ incident tsunami.

Wave rays were computed from a number of assumed incident directions by solving the wave geometric optic equation, and radar cells aligned along selected individual wave rays were identified (Fig. 4). Tsunami propagation times between such cells are computed based on the long wave phase velocity, as a function of the local bathymetry. For the calculation presented here, 2 single rays were selected (labeled by number 225 and 285 in Fig 4).

The reference of time ($t = 0$) corresponds to the initiation of the tsunami wave train at the source. Time is then measured onwards from this initial event. It takes approximatively 2 hours and 20 min for this tsunami to reach the shore of Vancouver Island near Tofino, BC (see Fig 5).

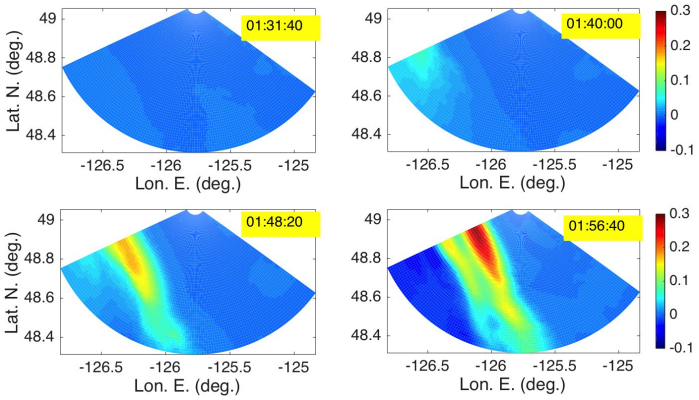

Fig. 5: Snapshot of tsunami radial current signed magnitude U_{tr}, simulated for the SSZ far-field seismic tsunami (Fig. 1) in the radar sweep area (color scale is in m/s). Yellowed numbers indicate propagation times from the tsunami source.

RADAR TIME SERIES

In earlier work (Grilli et al., 2016b, 2017), a numerical validation of the TCA detection algorithm was performed for the simulated SSZ tsunami (Figs. 1,4, 5), on the basis of numerically simulated radar signals using a radar simulator parameterized using the main characteristics of the actual WERA HF radar system in Tofino. The conclusion was that the TCA algorithm had the potential to detect the incoming tsunami further offshore, in deeper water, than using an algorithm based on currents directly inverted from the Doppler spectra. Despite these encouraging results, no definitive conclusions could be drawn before the TCA algorithm was tested with actual field radar data, which is the object of this paper. Indeed, besides the idealization of the radar signal in the simulator, particularly its decay and SNR with range, the background oceanic currents have also been idealized in this earlier work and ionospheric contamination as well as RFI ignored.

While it is impossible to generate a real tsunami on demand and see its impact on radar data, one can, however, numerically simulate the effect of a synthetic current, including from a tsunami, on a measured radar signal. This technique was already used for instance in (Gurgel et al., 2011) to simulate a past tsunami event and simulate the effect it would have produced on actual radar data. If not a definitive assessment of an operational TCA detection algorithm, this approach, which will be pursued here, represents a further step towards a more realistic simulator and a better evaluation of the detection algorithm performance.

To this aim, large amounts of raw signal recorded by the Tofino HF radar system, at a sampling rate $\Delta t = 0.26$ s, were obtained and processed in range and azimuth, using the software developed by Helzel Messtechnik GmbH, to produce time series of the complex backscattered signal $V_p(t)$ for each radar cell q (Fig. 4). Within this data, a few complete days of records were processed that represented different oceanic conditions.To simulate the impact of the computed tsunami on the radar data, we multiplied the latter by the complex memory term from Eq. (2), i.e.:

$$V_p^{tsu}(t) = V_p(t)\, e^{iM(t)} \tag{6}$$

To avoid spurious values sometimes observed in the radar signal time series and to equalize their magnitude at different ranges, only the re-centered and normalized complex values of the radar signal time series were retained, i.e., we considered signals of the form:

$$S_p(t) = \frac{V_p(t) - \overline{V_p}}{|V_p(t)|},\ S_p^{tsu}(t) = \frac{V_p^{tsu}(t) - \overline{V_p^{tsu}}}{|V_p^{tsu}(t)|} \tag{7}$$

where $\overline{V_p}$ and $\overline{V_p^{tsu}}$ are the temporal means of the signals (without and with tsunami) in the window of observation.

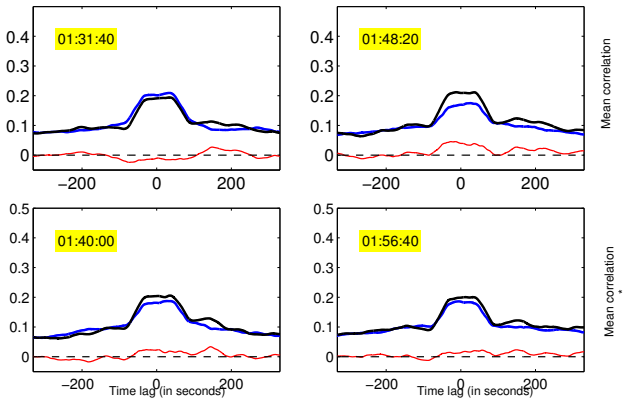

Fig. 6: Mean correlation $C_{30,6,2}$ calculated along wave ray 225 (Fig. 4) for original radar data from day 238 (i.e., in the absence of a tsunami). The blue and black solid lines represent the same function computed at 30 min intervals, the red solid line is the difference between these, which departs weakly from zero (marked by dashed black line). A very stable pattern is observed for 4 different reference times (yellowed labels).

Radar signal correlations were calculated based on $S_p^{tsu}(t)$ between pairs of cells (p,q) and referred to as $C_{pq}(\tau;t)$ and $C_{pq}^{tsu}(\tau;t)$, whether computed using the actual radar signal S_p, without a tsunami, or the modified signal S_p^{tsu}, simulating the presence of a tsunami. In each case, we correlated the signal at radar cell p with that at its Mth neighbor, $p+M$, for N successive values (that is $p = p_0, p_0+1, .., p_0+N-1$). The N resulting correlations were normalized by their maximum and averaged over the N available pairs:

$$C_{p_0,N,M}(\tau;t) = \frac{1}{N}\sum_{p=p_0}^{p_0+N-1} \frac{C_{p,p+M}(\tau;t)}{\max_\tau(C_{p,p+M}(\tau;t))} \tag{8}$$

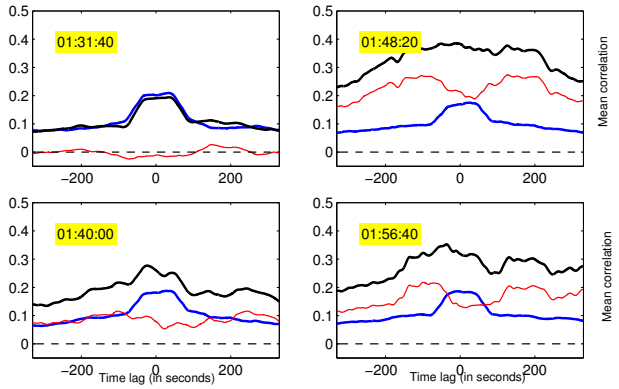

Fig. 7: Mean correlation calculated along wave ray 225 (Fig. 4) for day 238, $C_{30,6,2}$ (blue solid line) original data 30 min before tsunami arrival, and $C_{30,6,2}^{tsu}$ (black solid line), with tsunami superimposed on the radar data; 6 pairs of radar cells in the middle range (30-35 combined with 32-37) were used. The difference correlation (red solid line) clearly increases above some positive threshold as the tsunami wave train reaches the radar cells.

A further smoothing in time was finally applied to remove higher-frequency oscillations in average correlation. The function $C_{p_0,N,M}^{tsu}(\tau;t)$, in the presence of the tsunami, is defined in a similar way as in Eq. (8). The mean correlations $C_{30,6,2}$ and $C_{30,6,2}^{tsu}$ were computed along the 2 tsunami wave rays marked in Fig. 4, using the radar cells numbered 30 to 35 (corresponding to distances/radar ranges from 45 to 52.5 km) and correlating them with neighboring cells 2 up (i.e., cells 37 to 42), using an integration window $T_c = 900$ s and a smoothing window of 120 sec. Several days of radar data corresponding to different meteo-oceanic conditions were tested.

First, we evaluated the average correlation function $C_{30,6,2}(\tau;t)$ for the original radar data, using two times series separated by 30 min. Fig. 6 shows an example for a sequence of 25 min of original radar data extracted from day 238. Note that the observed correlation remains very stable in time, when considering the 4 reference times marked on the subplots. Next, we computed the average correlation function $C_{30,6,2}^{tsu}(\tau;t)$ in the presence of the simulated tsunami, where the first time series of complex radar signal was thus multiplied by the additional phase shift due to the tsunami current memory term (Eq. (7)), while the second time series (30 min before tsunami arrival) was kept unchanged. Fig. 7 shows a clear increase of the mean correlation $C_{p_0,N,M}^{tsu}$ at the time where the tsunami wave train reaches the radar cells. Again, this is due to the very coherent structure of the memory term across time and space, resulting in a high degree of correlation once the signal has been shifted by the appropriate propagation time between radar cells located along the same wave ray.

By contrast with the idealized case developed in Grilli et al. (2016a,b), where the radar data showed a flat correlation in the absence of the tsunami, here the correlation of the time-shifted radar data, $C_{pq}(\tau;t)$ exhibits a strong peak in correlation near the zero time lag, even in the absence of tsunami. This is an artifact of the preexisting cross-correlation of the radar signals simultaneously recorded at neighbor cells, likely due to the broadening of the range cell by the filtering window used for range discrimination in the range finding algorithm processing the raw radar data. This can be seen in Fig. 8, which plots the normalized cross-correlation of the radar signals calculated different radar cells (here from cells 30 to 36), for different values of M (here 0,2,4,6):

$$\frac{\mathrm{corr}\{S_p(t+\tau), S_{p+M}(t)\}}{\mathrm{corr}\{S_p(t), S_p(t)\}} \tag{9}$$

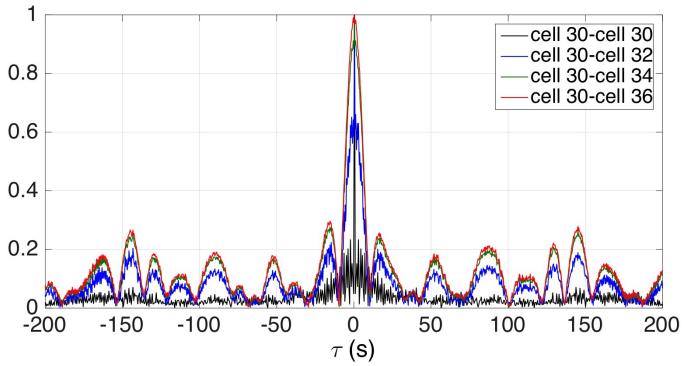

Fig. 8: Self-correlation in time of the radar signal calculated along wave ray 225 (Fig. 4), in the absence of a tsunami current, at cell 30 and its cross-correlation with neighboring cells 32, 34 and 36. A marked peak is observed at the zero time lag, even for the farthest apart cells.

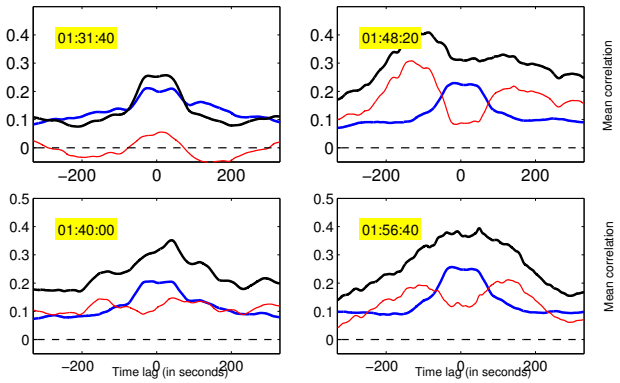

Fig. 9: Same as Fig. 7 for day 227.

A marked peak in correlation is visible, even when the radar cells are far apart. Since the propagation time t_{pq} between neighboring cells is smaller than the integration time used in Eq. (4), there is an overlap in the time intervals $[t_p - T_c/2, t_p + T_c/2]$ and $[t_q - T_c/2, t_q + T_c/2]$, which yields a peak of the correlation at the time lag $\tau = -t_{pq}$.

However, even though the time-shifted correlation in Eq. (4) is not flat in the absence of the tsunami, the occurrence of the latter manifests itself through a clear increase of the mean correlation $C_{p_0,N,M}$, due to highly correlated structure of the memory term caused by the tsunami current for time-shifted radar cell time series. Hence, tsunami detection is easily achieved, by observing a clear change of pattern of the mean correlation with respect to some reference function. In an operational way, the reference correlation for a given sea state in the absence of tsunami could be simply obtained from the radar signal recorded in the recent past, say, the previous 30 or 60 min of data, in such a way that the sea state and the radar characteristics can be assumed to be quasi-steady while the tsunami wave train has not yet reached the radar cells.

To further confirm these observations, Fig. 9 shows correlations similar to those computed for day 238 in Fig. 7, computed for another day of data, day 227. In both cases for days 227 and 238, tsunami detection could be achieved at time 1h40 by observing similar changes in pattern of the mean correlation, in the corresponding subplots of Fig. 7 and 9 (in fact at 1h40 + 450 s = 1h47 as one should account for the half the integration time window $T_c = 900$ sec). Such tsunami detection would thus take place about 30 min before tsunami arrival at the shore. Note that in using cells 30 to 35, detection was made possible based on the effect on correlation of fairly weak tsunami currents, simulated at the border of

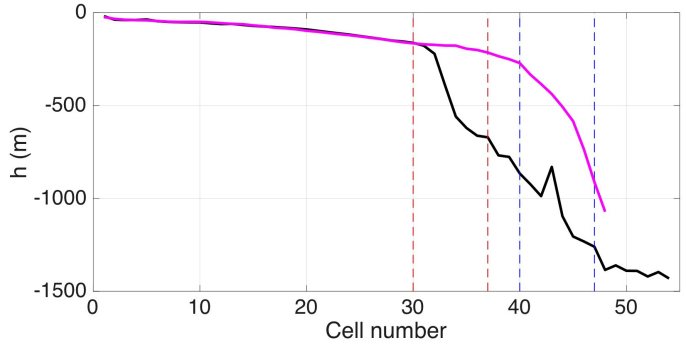

Fig. 10: Bathymetry along wave rays 225 (black) and 285 (magenta), used for validating the tsunami detection algorithm. The dashed vertical lines indicate the intervals of radar cells under consideration for middle-range (cells 30-37, red) and far-range (blue) detection.

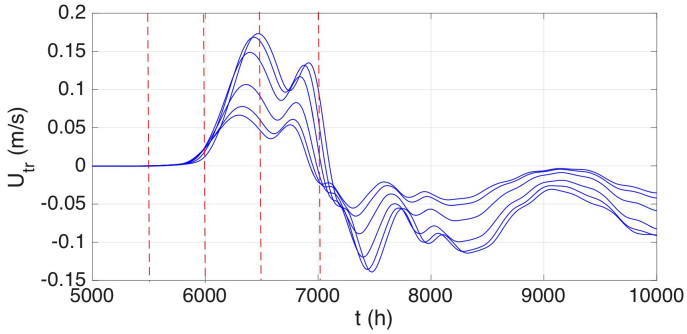

Fig. 11: Time series of cell-averaged tsunami radial currents (time is measured from the start of the SSZ event), at 6 cells 30 to 35, along wave ray 225 (Fig. 4). In the various curves, a decreasing current magnitude corresponds to an increasing range and hence cell number. The red dashed lines mark the 4 times of observations used in the subplots of Figs. 6, 7 and 9.

the continental shelf (see Fig 10). At these cells and in the time interval around the detection time, the cell-averaged radial tsunami currents are about 5 to 15 cm/s (see Fig 11).

In view of on these results, in an operational tsunami detection algorithm based on TCA, a detection criterion could thus be developed based on observing a marked positive difference between, ΔC, between the current time mean correlation $C^{tsu}_{p_0,N,M}$ and a reference mean correlation obtained from the recent past (e.g., 30 min earlier), which can be permanently computed and archived. A warning could thus be issued when ΔC increases above a to be defined threshold. For this a thorough statistical analysis based on extensive numerical simulations over a large number of days will be necessary in order to establish a related probability of detection.

It is expected that the detection performance of the algorithm can be improved by considering multiple wave rays and cells, and combining the corresponding correlations in some way. This is an entire new analysis, which remains to be done, but to verify this expectation, Fig. 12 shows the same correlation functions plotted at the same 4 times on day 238 using the wave ray labeled 285 in Fig. 4, rather than ray 225 as before. The continental shelf extends farther along this ray than along the previously considered ray 225 (see Fig. 10) , hence the induced tsunami currents reach a stronger magnitude for larger ranges than in the previous case. We see that detection would again occur at 1h40 min along this ray, based on the correlation threshold criterion.

We now compare the results of the TCA-based detection algorithm with what would be achievable with the same data using the classical de-

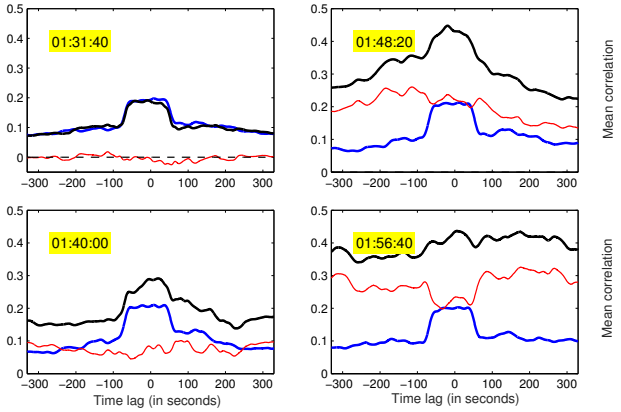

Fig. 12: Same as Fig. 7 for ray 285. The change in correlation pattern with and without a tsunami are more drastic due to the stronger tsunami currents along this ray.

tection method based on the Doppler spectrum. The range-Doppler maps obtained for the same radar time series along the same ray 225, with tsunami superimposed to the data, are plotted in Fig. 13 for the same 4 reference times, using an integration time of 2 min (note, this small integration time is acceptable considering the new method developed for processing Doppler spectra used here). While small deformations of the Bragg lines are indeed visible at times 1h48 and 1h56, it is difficult to discriminate those from the natural oscillations due to the spatial variations of the background current and not knowing that they are there, one would not be able to identify these and invert for the tsunami currents.

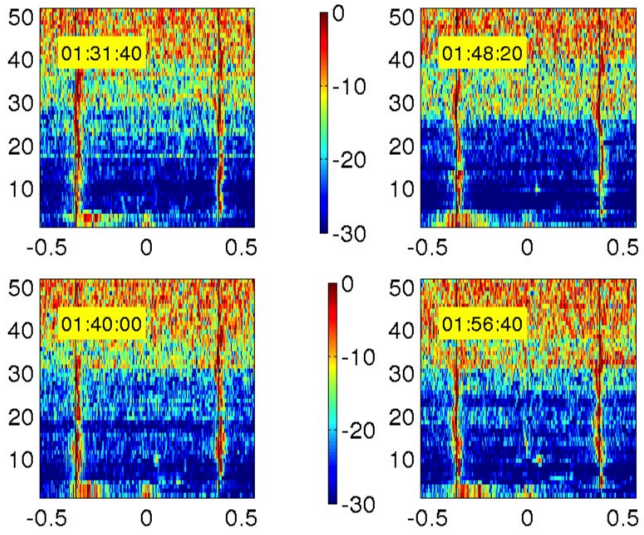

Fig. 13: Range-Doppler maps for the same radar data (with superimposed tsunami) as in Fig 8 (day 238), with cell numbers on the vertical axis. A small deformation of the Bragg lines is visible at times 1h48 and 1h56 but is difficult to discriminate from the natural oscillations due to the spatial variations of the background current.

BEYOND THE SHELF DETECTION

We finally tested the sensitivity of the TCA detection algorithm to range, and hence current magnitude, by the farthest radar cells, which are well beyond the continental shelf, with corresponding water depths of 1,000 m or more (Fig. 10). We thus recomputed the same mean correlations as plotted in Figs. 7 and 9 for days 238 and 227, using the radar data, with superimposed (weaker) tsunami currents, of cells 40 to 45 combined with cells 42 to 47. Results in Figs. 14 and 15 show the evolution of the mean correlation $C^{tsu}_{40,6,2}$ during the propagation time of the tsunami. A small but clear overall increase of this function can still be seen, as the tsunami reaches the selected cells (around 1h40). The lesser values of the contrast ΔC, as compared to the middle range cell case ($C^{tsu}_{30,6,2}$), could lead to false alarms. However, this correlation jump could be reinforced by considering multiple wave rays, and in any case this could serve to issue an initial warning, to be confirmed once the tsunami reaches the middle cell range, where currents become larger and the correlation contrast becomes higher.

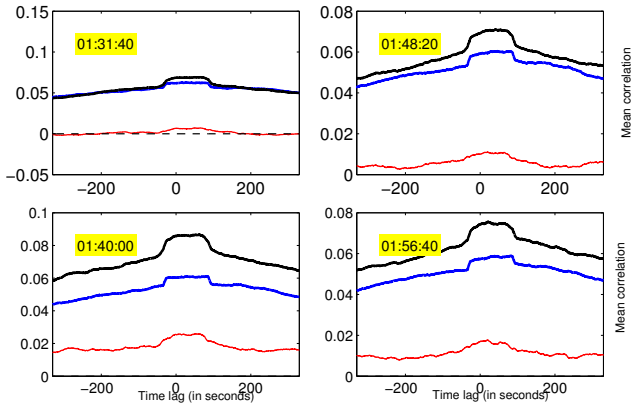

Fig. 14: Mean correlation calculated along wave ray 225 (Fig. 4) for day 238, $C_{40,6,2}$ (blue solid line) original data 30 min before tsunami arrival, and $C^{tsu}_{30,6,2}$ (blue solid line), with tsunami superimposed on the radar data; 6 pairs of radar cells in the middle range (40-45 combined with 42-47) were used. Even though the difference correlation (red solid line) is small in absolute value, there is a clear increase above some positive threshold as the tsunami wave train reaches the radar cells.

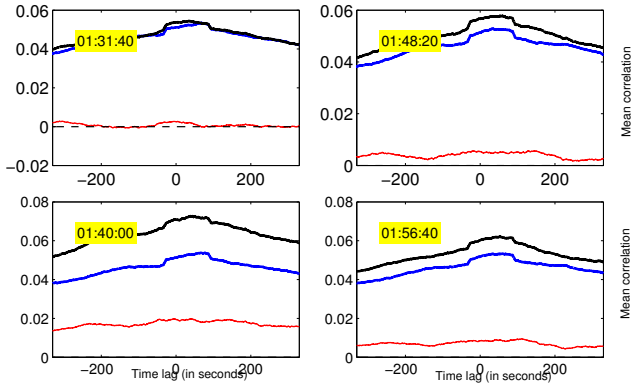

Fig. 15: Same as Fig. 14 for day 227.

CONCLUSIONS

We tested the TCA algorithm for early tsunami detection proposed and validated in our earlier work purely based on numerical simulations (Grilli et al., 2016b, 2017), using for the first time actual radar data measured by the ONC WERA HF radar deployed at Tofino, BC, on the Pacific Ocean side of Vancouver Island. The effect of an incoming tsunami

(from a M_w 9.1 far field seismic tsunami originating in the Semidi Subduction Zone), simulated using a state-of-the-art long wave model, is superimposed onto the experimental HF radar data by way of a current memory term; this method that has been used and validated in HF radar papers published by other groups (e.g. (Gurgel et al., 2011)).

A detection method was developed that compares mean correlations of radar signal from various radar cells, time shifted by the tsunami propagation time along precomputed wave rays; a marked increase in the pre-existing correlation (say 30 min in the past) indicates that a tsunami is propagating into the radar sweep area. Results obtained so far are very promising and confirm the predictions made in our earlier work that the TCA algorithm has the potential for detecting a tsunami in deeper water, beyond the continental shelf, where tsunami-induced currents are small (as low as 5 cm/s), than when using an algorithm based on a direct inversion of currents from the measured radar Doppler spectra.

Further tests and improvements are in progress, whose results will be presented at the conference.

Acknowledgements The authors thank the company Helzel Messtechnik GmbH (in particular Dr. A. Dzvonkovskaya) for technical support to process the radar data and Ocean Network Canada for the WERA data and support to the University of Rhode Island to conduct this research. C.-A. Guérin also acknowledges the CNRS, the University of Toulon and the French-American Fulbright commission for supporting his sabbatical leave at URI.

REFERENCES

Benjamin, L. R., Flament, P., Cheung, K. F., and Luther, D. S. (2016). The 2011 Tohoku tsunami south of Oahu: high-frequency Doppler radio observations and model simulations of currents. *J. Geophys. Res. (publ. online)*, pages 1–29.

Dzvonkovskaya, A. (2012). Ocean surface current measurements using HF radar during the 2011 Japan tsunami hitting Chilean coast. In *Geoscience and Remote Sensing Symp. (IGARSS), 2012 IEEE Intl.*, pages 7605–7608. IEEE.

Dzvonkovskaya, A., Gurgel, K.-W., Pohlmann, T., Schlick, T., and Xu, J. (2009). Simulation of tsunami signatures in ocean surface current maps measured by HF radar. In *OCEANS 2009-EUROPE*, pages 1–6. IEEE.

Grilli, S., Shelby, M., Grilli, A., Guérin, C.-A., Grosdidier, S., and Insua, T. (2017). Tsunami detection by High Frequency Radar beyond the continental shelf: II. Extension of algorithms and validation on realistic case studies. *Pure and Applied Geophysics submitted*.

Grilli, S. T., Grosdidier, S., and Guérin, C.-A. (2016a). Tsunami detection by High Frequency Radar beyond the continental shelf. I. Algorithms and validation on idealized case studies. *Pure and Applied Geophysics*, 173(12):3,895–3,934.

Grilli, S. T., Shelby, M., Grilli, A., Guérin, C.-A., Grosdidier, S., Insua, T., et al. (2016b). Algorithms for tsunami detection by high frequency radar: Development and case studies for tsunami impact in british columbia, canada. In *The 26th International Ocean and Polar Engineering Conference*, pages pps. 807–814. International Society of Offshore and Polar Engineers.

Gurgel, K.-W., Dzvonkovskaya, A., Pohlmann, T., Schlick, T., and Gill, E. (2011). Simulation and detection of tsunami signatures in ocean surface currents measured by HF radar. *Ocean Dynamics*, 61(10):1495–1507.

Heron, M. L., Prytz, A., Heron, S. F., Helzel, T., Schlick, T., Greenslade, D. J., Schulz, E., and Skirving, W. J. (2008). Tsunami observations by coastal ocean radar. *International Journal of Remote Sensing*, 29(21):6347–6359.

Hinata, H., Fujii, S., Furukawa, K., Kataoka, T., Miyata, M., Kobayashi, T., Mizutani, M., Kokai, T., and Kanatsu, N. (2011). Propagating tsunami wave and subsequent resonant response signals detected by HF radar in the Kii Channel, Japan. *Estuarine, Coastal and Shelf Science*, 95(1):268–273.

Insua, T., Grilli, A. R., Grilli, S. T., Shelby, M., Wang, K., Gao, D., Cherniawsky, J., Harris, J. C., Heesemann, M., McLean, S., and Moran, K. (2015). Preliminary tsunami hazard assessment in British Columbia, Canada. *EOS Trans. AGU*, 96(52):Fall Meet. Suppl., Abstract NH23C–1890.

Lipa, B., Barrick, D., Saitoh, S.-I., Ishikawa, Y., Awaji, T., Largier, J., and Garfield, N. (2011). Japan tsunami current flows observed by HF radars on two continents. *Remote Sensing*, 3(8):1663–1679.

Lipa, B., Isaacson, J., Nyden, B., and Barrick, D. (2012). Tsunami arrival detection with high frequency (HF) radar. *Remote Sensing*, 4(5):1448–1461.

Lipa, B. J., Barrick, D. E., Bourg, J., and Nyden, B. B. (2006). HF radar detection of tsunamis. *Journal of Oceanography*, 62(5):705–716.